Biochemistry. In the article "Characterization of recombinant phytochrome from the cyanobacterium *Synechocystis*" by Tilman Lamparter, Franz Mittmann, Wolfgang Gärtner, Thomas Börner, Elmar Hartmann, and Jon Hughes, which appeared in number 22, October 28, 1997, of *Proc. Natl. Acad. Sci. USA* (**94,** 11792–11797), a name appeared incorrectly in the acknowledgments on page 11797 due to a printer's error. Prof. Silvia Braslavski (Max-Planck-Institut für Strahlenchemie, Mülheim) should be listed as Prof. Silvia Braslavsky.

Neurobiology. In the article "β subunits influence the biophysical and pharmacological differences between P- and Q-type calcium currents expressed in a mammalian cell line" by Herman Moreno, Bernado Rudy, and Rodolfo Llinás, which appeared in number 25, December 9, 1997, of *Proc. Natl. Acad. Sci. USA* **94,** 14042–14047, the following correction should be noted. Due to an editorial change at PNAS, the meaning of the last sentence on page 14046 was altered. The sentence originally read as follows: On the other hand, this structure does not reproduce the pharmacological properties of either P or Q channel exactly, as the ID_{50} to sFTX and ω-Aga IVA for P-type channels is lower than for the α1A, $\alpha 2\delta$, βIb channels in HEK cells.

Neurobiology. In the article "The synthesis of ATP by glycolytic enzymes in the postsynaptic density and the effect of endogenously generated nitric oxide" Kuo Wu, Chiye Aoki, Alice Elste, Adrienne A. Rogalski-Wilk, and Philip Siekevitz, which appeared in number 24, November 25, 1997, of *Proc. Natl. Acad. Sci. USA* (**94,** 13273–13278), the quality of the reproduction of Fig. 2A was poor. The figure and its legend are shown below:

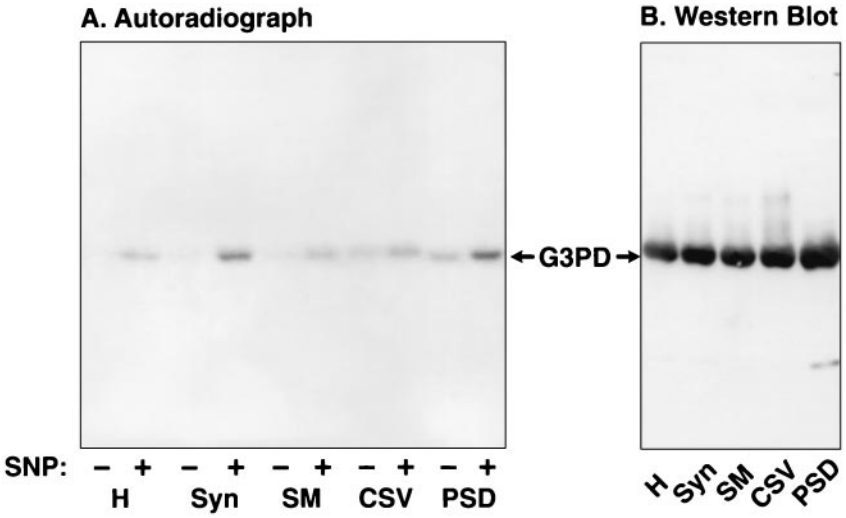

FIG. 2. (*A*) NO-stimulated [adenylate-^{32}P]NAD incorporation into G3PD in subcellular fractions isolated from adult porcine cerebral cortex. Assays are described in *Materials and Methods*. PSD (50 μg) and 100 μg each of the other fractions, in 100 μl final volume, including whole homogenate (H), synaptosomes (Syn), synaptic plasma membranes (SPM), and crude synaptic vesicles (CSV), were incubated at 37°C for 15 min. NAD incorporation was performed in the absence (−) or presence (+) of SNP as exogenous source of NO. The mixtures were subjected to SDS/PAGE and then autoradiography. (*B*) Western blot analysis of the G3PD in the subcellular fractions. To confirm that the radioactive protein in the subcellular fractions was indeed G3PD, Western blot analysis was performed by using specific anti-G3PD antibodies as described.

Biochemistry. In the article "KSR stimulates Raf-1 activity in a kinase-independent manner" by Neil R. Michaud, Marc Therrien, Angela Cacace, Lisa C. Edsall, Sarah Spiegel, Gerald M. Rubin, and Deborah K. Morrison, which appeared in number 24, November 25, 1997, of *Proc. Natl. Acad. Sci. USA* (**94,** 12792–12796), the following correction should be noted. Due to a printer's error, background was incorrectly added to Fig. 2 *A* and *B* on page 12793, Fig. 3*B* on page 12794, and Fig. 4 *A–C* on page 12795 so that multiple panels from different gels or Western blots appear as one continuous panel. Correct versions of Figs. 2, 3, and 4 and each figure legend are reproduced here and on the opposite page.

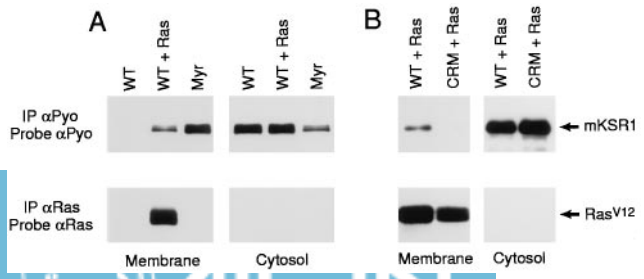

FIG. 2. The mKSR1 CA3 domain is required for the Ras-dependent membrane localization of mKSR1. (*A*) 293 cells transiently expressing WT and Myr mKSR1 or coexpressing WT and Ras^{V12} were fractionated into membrane and cytosolic fractions. The mKSR1 proteins were immunoprecipitated and examined by immunoblot analysis using αPyo antibody. (*B*) 293 cells coexpressing Ras^{V12} and either WT or CRM mKSR1 proteins were analyzed as in *A*.

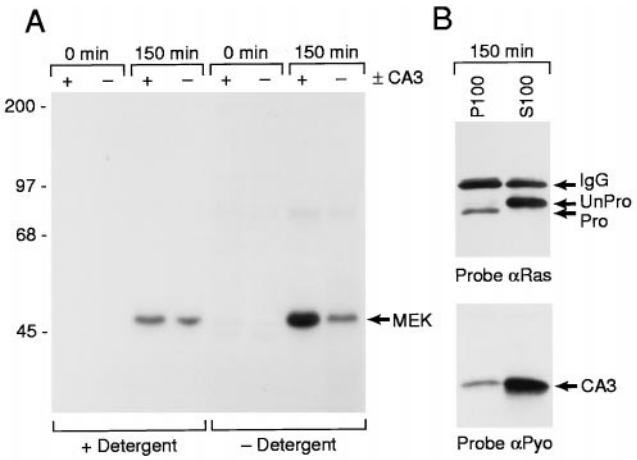

FIG. 3. The mKSR1 CA3 domain augments Raf-1 activity in a detergent-sensitive manner. *Xenopus* oocytes expressing Raf-1 alone (−) or coexpressing Raf-1 and the mKSR1 CA3 domain (+) were injected with Ras^{V12} RNA. Immediately after (0 min) or 150 min after Ras^{V12} injection, oocytes were lysed in hypotonic buffer and membranes were isolated. (*A*) Raf-1 proteins were immunoprecipitated from membrane fractions resuspended in RIPA buffer (+ detergent) or phosphate-buffered saline (− detergent), and *in vitro* kinase assays were performed using kinase-inactive MEK as a substrate (1). Phosphorylation of MEK1 on Ser-218 and Ser-222 was determined by tryptic peptide mapping analysis. (*B*) Ras^{V12} and CA3 proteins were immunoprecipitated from membrane (P100) and cytosolic fractions (S100) isolated at 150 min after injection with Ras^{V12} RNA and were examined by immunoblot analysis using Ras and Pyo antibody, respectively. The migration of processed (Pro) and unprocessed (UnPro) Ras proteins is indicated.

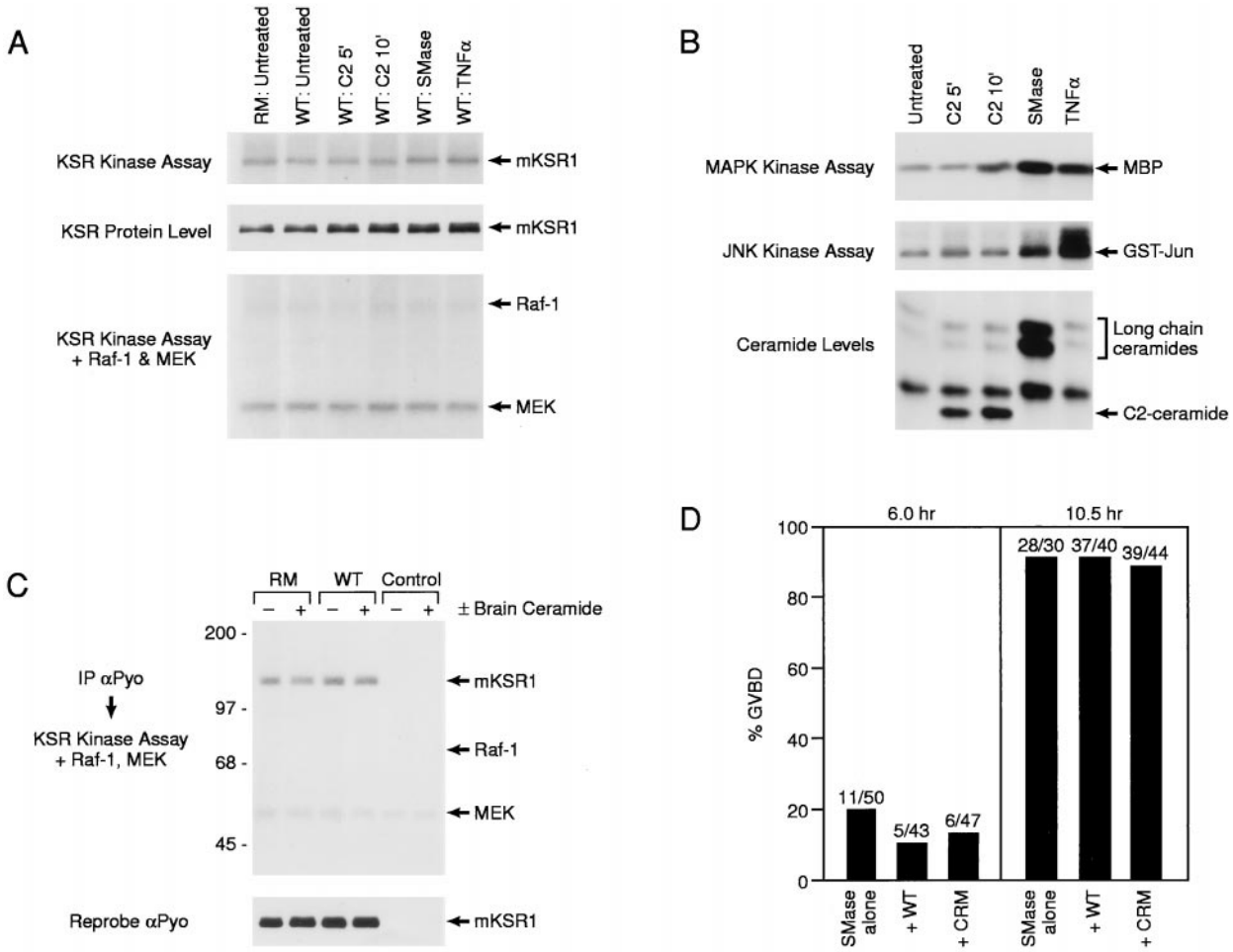

FIG. 4. Augmentation of Ras signaling by mKSR1 does not involve ceramide. (*A*) Cos cells were transiently transfected with constructs encoding wild-type (WT) or kinase-inactive (RM) mKSR1. At 60 hr posttransfection, serum starved cells were left untreated or were stimulated with 20 μM C2 ceramide for 5 or 10 min, 100 milliunits/ml sphingomyelinase (SMase) for 20 min or 10 nM tumor necrosis factor α (TNFα) for 20 min. KSR proteins were immunoprecipitated using αPyo antibody, and mKSR1 immune complex kinase assays were performed *in vitro* as described by Zhang *et al.* (ref. 19; *Top*). Immunoprecipitated mKSR1 was detected by immunoblot analysis (*Middle*). To observe phosphorylation of Raf-1 or modulation of Raf-1 activity, purified activated Raf-1, coexpressed in Sf9 cells in the presence of RasV12 and v-src, and kinase-inactive MEK1 were added to the mKSR1 immune complex kinase assays previously described (ref. 19; *Bottom*). (*B*) Cos cells were treated as in *A* and endogenous ceramide levels, JNK activity, and MAPK activity were determined. Ceramide levels were normalized to the untreated control. C2-ceramide levels were elevated 2.9- and 3.7-fold at 5 and 10 min, respectively, and long-chain ceramide levels were elevated 12-fold by SMase and 1.9-fold by TNFα. (*C*) Purified brain ceramide (100 nM) (+) or diluent (−) was added *in vitro* to mKSR proteins immunoprecipitated from transfected Cos cells and immune complex kinase assays performed in the presence of activated Raf-1 and kinase-inactive MEK1 as previously described (ref. 19; *Top*). Immunoprecipitated mKSR1 was detected by immunoblot analysis (*Bottom*). (*D*) Oocytes preinjected with buffer or RNA encoding WT and CRM mKSR1 constructs were treated with 250 milliunits sphingomyelinase. GVBD was then scored 6 and 10.5 hr after treatment.

Proc. Natl. Acad. Sci. USA
Vol. 94, pp. 14042–14047, December 1997
Neurobiology

β subunits influence the biophysical and pharmacological differences between P- and Q-type calcium currents expressed in a mammalian cell line

(human epithelial kidney cells/voltage-gated calcium channels/coexpression/Purkinje cells)

HERMAN MORENO*, BERNARDO RUDY*†, AND RODOLFO LLINÁS*‡

Departments of *Physiology and Neuroscience and †Biochemistry, New York University Medical Center, 550 First Avenue, New York, NY 10016

Contributed by Rodolfo Llinás, October 22, 1997

ABSTRACT **Human epithelial kidney cells (HEK) were prepared to coexpress α1A, α2δ with different β calcium channel subunits and green fluorescence protein. To compare the calcium currents observed in these cells with the native neuronal currents, electrophysiological and pharmacological tools were used conjointly. Whole-cell current recordings of human epithelial kidney α1A-transfected cells showed small inactivating currents in 80 mM Ba^{2+} that were relatively insensitive to calcium blockers. Coexpression of α1A, βIb, and α2δ produced a robust inactivating current detected in 10 mM Ba^{2+}, reversibly blockable with low concentration of ω-agatoxin IVA (ω-Aga IVA) or synthetic funnel-web spider toxin (sFTX). Barium currents were also supported by α1A, β2a, α2δ subunits, which demonstrated the slowest inactivation and were relatively insensitive to ω-Aga IVA and sFTX. Coexpression of β3 with the same combination as above produced inactivating currents also insensitive to low concentration of ω-Aga IVA and sFTX. These data indicate that the combination α1A, βIb, α2δ best resembles P-type channels given the rate of inactivation and the high sensitivity to ω-Aga IVA and sFTX. More importantly, the specificity of the channel blocker is highly influenced by the β subunit associated with the α1A subunit.**

After the initial description of P-type calcium channels in Purkinje cells (1, 2), and the subsequent designation of the Q-type calcium channels as a separate channel category (3), concern has arisen regarding their true distinctness. The issue at hand concerns the use of pharmacological or biophysical operational definitions as a sole requirement in channel characterization, especially given the functional significance of these moieties in central nervous system physiology and pathology. Indeed, the molecular elements for the native P- and Q-type channels remain unclarified (4, 5).

Presently the accepted nomenclature for voltage-gated calcium channels include L, N, P, Q, R, and T. These channels are multimeric structures consisting of a main pore-forming subunit (α1), which can implement calcium ion conductance on its own in heterologous expression systems (5, 6). In addition, two other subunits are important in the functioning of the channel, α2δ and β (7, 8). It has been shown that the α2δ subunit increases the amount of α1C subunit (L-type calcium channel) at the plasmalemma, whereas β subunits increase the opening probability of the calcium channels expressed by the α1C subunit (9). In the case of P- and Q-type channels it has been proposed, based on pharmacology (5, 10), molecular dissection experiments (11), and subcellular localization (12, 13), that the α1A subunit is the pore-forming component. Given that this subunit does not reproduce the functional properties of P and Q calcium currents on its own, we tested whether different β subunits in the presence of the constant α2δ subunit produced any differences in the electrophysiological and/or pharmacological properties of α1A currents in a mammalian expression system.

MATERIALS AND METHODS

Preparation of Human Epithelial Kidney (HEK) Cells Expressing Channel Proteins. For transient expression of channel proteins, HEK 293T cells were grown in DMEM (GIBCO) supplemented with 10% fetal bovine serum, 100 units/ml of penicillin G, and 100 μg/ml of streptomycin (GIBCO), and plated at 50% confluence. The appropriate cDNAs (α1A, α2δ, βIb, β2a, β3, and green fluorescence protein) were subcloned into the mammalian expression vector pcDNA 3.1 (Invitrogen). All calcium channels subunits were a kind gift of T. Snutch (University of British Columbia, Vancouver). Green fluorescence protein was obtained from CLONTECH. Cells expressing channels were prepared by using DOTAP (Boehringer Mannheim) to introduce the recombinant vectors (1 μg each) by lipofection according to the manufacturer's protocols. After transfection, cells were allowed to reach 70% confluence and then plated at a 1:5 ratio and recorded 8–24 hr later.

Electrophysiological Analysis. Whole-cell recordings (14) were obtained from green fluorescent cells, which were observed with an excitation wavelength of 488 nM and emission of 515 nM at room temperature by using an Axopatch 200-A (Axon Instruments, Foster City, CA). Cells were maintained in an extracellular solution containing 135 mM NaCl, 3.5 mM KCl, 1.5 mM $CaCl_2$, 1.0 mM $MgCl_2$, 5.0 mM glucose, and 10 mM Hepes (pH adjusted to 7.35 with NaOH). For the recording of barium currents the external solution contained 142 mM tetraethylammonium (TEA)-Cl, 10 mM $BaCl_2$, and 10 mM Hepes·CsOH (pH 7.35) "standard solution." Experiments with high extracellular barium used 80 mM $BaCl_2$, 12 mM TEA-Cl, 10 mM Hepes (TEA), 290 mOsm with sucrose, and liquid junction potential was measured and subtracted for generation of *I–V* plots (15). The patch clamp pipettes contained a solution of 110 mM $CsMeSO_4$, 4.5 mM $MgCl_2$, 10 mM EGTA, 8 mM ATP, and 10 mM Hepes (pH adjusted to 7.35 with CsOH) and showed resistances of 3–7 MΩ (typically 4 MΩ). Calcium currents were obtained in an extracellular solution of 40 mM $CaCl_2$, 80 mM TEA-Cl, 10 mM Hepes·CsOH (pH 7.35), 290 mOsm. For these experiments pipette solution contained 2.0 mM EGTA, otherwise identical to that described. Seal resistance was typically 10 GΩ. Recordings were obtained with partial series resistance compensation (60–80%), and most of the cell capacitance canceled. The currents were low pass-filtered at 2–5 kHz by using an eight pole Bessel filter

The publication costs of this article were defrayed in part by page charge payment. This article must therefore be hereby marked "*advertisement*" in accordance with 18 U.S.C. §1734 solely to indicate this fact.

Abbreviations: HEK, human epithelial kidney cells; sFTX, synthetic funnel-web spider toxin; ω-Aga IVA, ω-agatoxin IVA.

‡To whom reprint requests should be addressed.

(Frequency Devices, Haverhill, MA) and digitized at 2.5–5 kHz. Subtraction of leak and remaining capacitance was obtained by using a P/4 protocol. For data acquisition and analysis and voltage clamp protocols we used the PCLAMP software (Axon Instruments). Drugs, as well as recording extracellular solutions, were applied locally by means of a blunt pipette (gravity flow). sFTX (1, 16, 17) was freshly prepared before using, and ω-Aga IVA (a gift from Pfizer) was stored at −20°C as stock solution (100 μM).

RESULTS

The Pharmacological Profile of the Current Expressed by α1A Subunit Varies Depending on its Associated β Subunit. The effects of sFTX and ω-Aga IVA on expressed calcium currents were examined in HEK 293T cells transiently transfected with α1A, α2δ cDNAs with and without different β subunits cDNAs. Green fluorescence protein was used to identify transfected cells. Expression of the different combinations resulted in Ba^{2+} currents with characteristic electrophysiological properties (Fig. 1) in whole-cell mode (see also ref. 5). When α1A subunits were coexpressed with α2δ and βIb they produced a fast-activating inward Ba^{2+} current sensitive to submillimolar concentrations of sFTX. The dose–response curve (Fig. 2*A*) shows a IC_{50} of 410 μM with a saturating maximum block around 1.5 mM. Interestingly, higher extracellular Ba^{2+} concentration (80 mM, concentration commonly used in single-channel studies) shifted the sFTX dose–response curve (Fig. 3 *C* and *D*). These results were consistent with studies that report Ba^{2+} ions concentration dependence

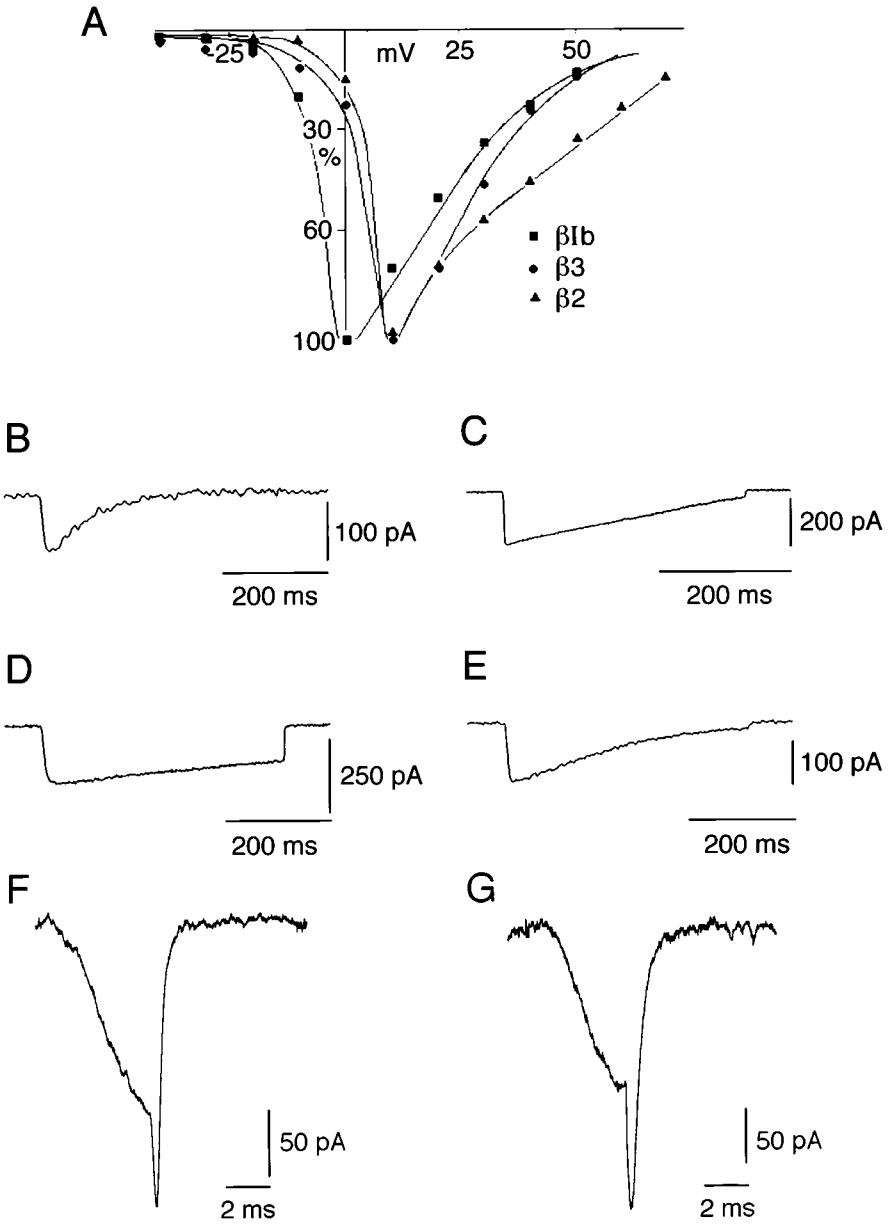

FIG. 1. Global properties of α1A calcium channel subunit expressed by itself and in combination with different β subunits in HEK (293T) cells. Current-voltage relations for α1A, α2δ, βIb (■), α1A, α2δ, β2a (▲), and α1A, α2δ, β3 (●). Currents were recorded in "standard" extracellular solution. (*A*) Macroscopic whole-cell barium currents of transiently transfected HEK cells expressing different calcium channel subunits combinations were observed. The barium currents elicited in response to depolarizing steps from a holding potential of −90 mV. α1A in 80 mM extracellular barium step to +20 mV (*B*), α1A, α2δ, βIb in "standard solution" step to +10 mV (*C*), α1A, α2δ, β2a (*D*), and α1A, α2δ, β3 (*E*) currents in response to the same protocol as in *C*. Tails currents of α1A, α2δ, and two different β subunits were generated from a pulse to + 10 mV and then step to −110 mV in 10 mV increments every 20 sec, shown are the recordings of tails generated at −80 mV for a α1A, α2δ, β2a (three averaged currents) (*F*) and α1A, α2δ, βIb (*G*).

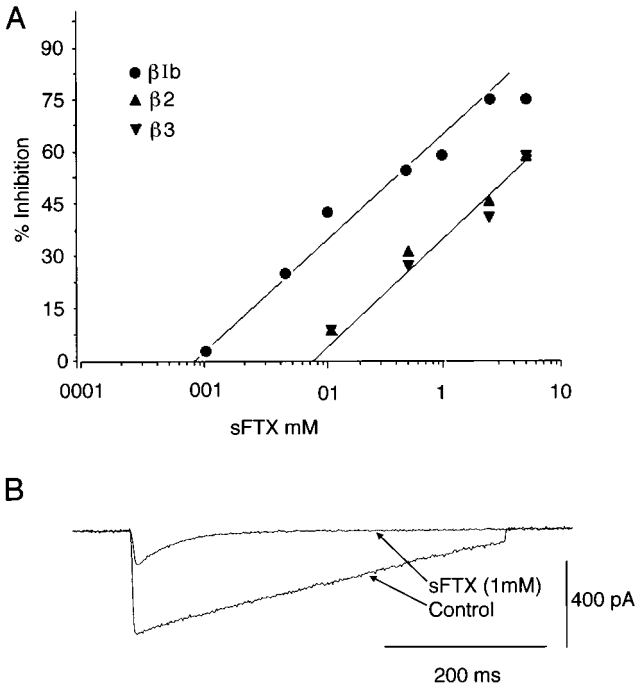

FIG. 2. sFTX effect on α1A, $\alpha2\delta$ currents vary depending on the β subunit coexpressed. Dose–response for α1A, $\alpha2\delta$, βIb currents (●), α1A, $\alpha2\delta$, β2a currents (▲), and α1A, $\alpha2\delta$, β3 currents (▼) at the noted sFTX concentrations locally applied through a blunt pipette. Note the difference in sensitivity between the currents produced in cells expressing βIb and the other two subunit combinations (*A*). α1A, $\alpha2\delta$, βIb whole-cell current using the same protocol as in Fig. 1*C*, before (control) and after 1 mM sFTX (sFTX 1 mM) (*B*). The effect of sFTX was observed within ~1 min, was reversible, and produced a noticeable difference in the τ of inactivation (see text).

on sFTX block of P-like calcium currents expressed in *Xenopus* oocytes (16).

The kinetics of the sFTX block was rather slow, with a transient but consistent increase of current seconds after local bath application, followed by maximum inhibition 1–4 min later. sFTX block reversed on washout and had a time course of ~20 sec, reaching a 60 +/− 15% of initial current in ~20 sec. Saturating concentrations of sFTX produced a significant decrease of τ inactivation (τ inactivation at +20 mV before sFTX = 233 +/− 12 msec and 43.64 +/− 7 msec after sFTX n = 4) (see Fig. 2*B*), resembling an open-channel blockade. Local application of ω-Aga IVA produced a significant block at a concentration higher than 50 nM (Fig. 4*A*). This effect was similar at low and high extracellular Ba^{2+} concentrations in contrast to the effect of sFTX (Fig. 3 *A* and *B*). The kinetics of ω-Aga IVA block (slow onset of its action) was comparable to those observed in hippocampal, dorsal root ganglion, and cerebellar granule neurons (18). Current inhibition produced by ω-Aga IVA was partially reversible on toxin withdrawal after 5–15 min. The percentage of recovery varied widely between cells and had values between 10% and 35%. The rate and amount of recovery was modified by high amplitude (+150 mV) depolarizing steps (1 Hz of 30 pulses of 50 msec duration). Under this protocol α1A, βIb, $\alpha2\delta$ currents recovered in 3–5 min to 40–55% of their initial value (Fig. 4*C*). This protocol has been shown to speed up recovery from ω-Aga IVA block for both P-type currents in cerebellar Purkinje cells and in α1A currents obtained by expression in *Xenopus* oocytes (2, 10).

Coexpression of α1A, β2a, $\alpha2\delta$ subunits were relatively insensitive to submillimolar concentrations of sFTX, obtaining a 40% block at 1 mM local application of the toxin, with similar on and off kinetics as that observed for the combination α1A, $\alpha2\delta$, βIb. ω-Aga IVA at 50 nM did not produce any significant effect on the barium currents produced by this subunit combination. Effects were clearly observed only at concentrations higher than 100 nM (Fig. 4*A*). For instance, 500 nM produced a 90% inhibition of this current (Fig. 4*B*). The inhibition was reversible in 60% of the cells reaching a 26 +/− 10% recovery 8–12 min after toxin withdrawal, which increased to 40 +/− 15% after high depolarizing prepulses as illustrated in Fig. 4*B*.

The response to sFTX of the currents obtained by α1A, $\alpha2\delta$, and β3 was similar to that of the α1A, $\alpha2\delta$, and β2a combination (Fig. 4*A*), with similar block characteristics as those observed for the other subunit combinations tested. ω-Aga IVA at 100 nM did not produce any significant effect on the current. In the absence of β subunits α1A currents were detectable only in high extracellular Ba^{2+}, and local application of sFTX produced a block only at high millimolar concentrations (~30% at 5 mM). No significant effects were observed at lower concentration. On the other hand, 200 nM ω-Aga IVA produced a 30 +/− 15% inhibition.

Contribution of β Subunits to the Electrophysiological Properties of α1A Currents. Expression of α1A, $\alpha2\delta$ calcium channel subunits in heterologous expression systems produced barium or calcium currents that varied in amplitude and inactivation depending on which β subunit is present (5, 9). We explored if the β subunits affect other electrophysiological properties of the α1A subunit. Whole-cell recordings of HEK α1A, $\alpha2\delta$, and βIb transfected cells showed inward barium currents first seen at (−20 mV) with a peak current at −10 to 0 mV with a fast-activating kinetics (time to peak = 2.4 +/− 0.4 msec n = 12) (Fig. 1 *A* and *C*). The potential at which half of the channels were activated was calculated from a smooth curve fitted to the raw *I–V* data ($I = G(xE)/\{1+\exp[(V\text{-}V_{1/2})/K]\}$ (V_{50} = 6.92 +/− 1.2 mV and e fold value = 2.8). Inactivation was studied by single long trace pulses as well as by instantaneous onset currents as shown in Fig. 5 *C* and *D*. Inactivation was best-fit by a single exponential in both protocols, which generated similar results, although the rate of inactivation was rather variable between cells (τ inact to + 20 mV = 225 +/− 64 msec n = 12) (Fig. 5 *C* and *D*). α1A, $\alpha2\delta$, βIb barium currents were relatively stable, and in some cases no rundown was observed (rundown 20 +/− 14% n = 12). Recovery from inactivation demonstrated a fast partial recovery, which was little affected over periods of seconds, reaching a 68 +/− 8% of initial value at 8 sec (Fig. 5*B*).

Attempts to study the currents with calcium as the main charge carrier produced a progressive current decay, reaching close to a complete block within ~6 min (Fig. 5*E*). Indeed, such current once having vanished in the presence of calcium, quickly returned in a Ba^{2+} environment. This result suggested that the α1A, $\alpha2\delta$, βIb channel protein complex undergoes calcium-induced calcium channel inhibition in a reversible fashion. Tail current analysis (n = 6) demonstrated a τ off rate to −80 mV = 0.57 +/− 0.07 msec, best-fit by a single exponential (Fig. 1*G*). α1A, $\alpha2\delta$, β2a produced a fast-activating I_{Ba} (time to peak = 2.26 +/− 0.6 msec) (Fig. 1*D*). This current also showed a high variability of the rate of inactivation; for instance, 50% of the cells (n = 14) did not inactivate during 500 msec whereas the rest of the cells had a τ inact at +20 mV = 860 +/− 300 msec, with a peak current at 0 to +10 mV (Fig. 1 *A* and *D*). Tail current to −80 mV was best-fit monoexponentially (τ off rate at −80 mV = 0.42 +/− 0.14 msec) (Fig. 1*F*).

Coexpression of the same α subunits with β3 subunit produced fast-activating (time to peak = 2.16 +/− 0.7 msec) currents inactivated with a τ inact to + 20 mV = 214 +/− 28 msec (n = 4) (Fig. 1 *A* and *E*). In the three combinations studied, α1A, $\alpha2\delta$, and the different β(s) calcium channel subunits, high extracellular Ba^{2+} (40–80 mM) produced a shift to the right of the *I–V* relationship (see Figs. 3 *A* and *C* and 5*A*).

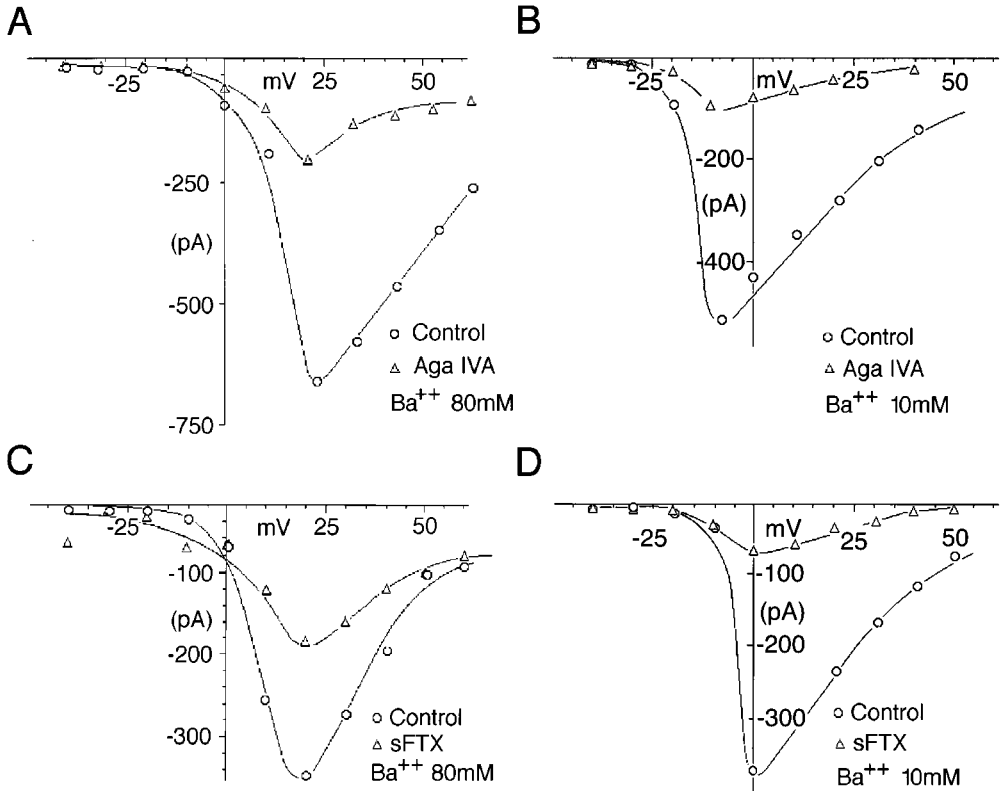

FIG. 3. sFTX but not ω-Aga IVA block of α1A, α2δ, βIb currents is affected by barium ions. *I–V* relations of α1A, α2δ, βIb before (control O) and after ω-Aga IVA (△) in 80 (*A*) and 10 mM barium (*B*), also shown same type of *I–V* relations before and after 1 mM sFTX (△) in 80 (*C*) and 10 mM barium (*D*). All recordings were performed by using the same protocol as in Fig. 1*C*. Voltage steps from −50 to + 40 mV in 10 mV increments were delivered every 20 sec. Recordings performed in high barium are shifted 10–20 mV to the right. This was true for all of the α1A, α2δ, β subunit combinations tested.

DISCUSSION

The present set of results address the issue of the differences between P and Q channels. The issue of what defines a channel type becomes one of the questions to be examined. Our results suggest that the P and Q channels are indeed functional variances of the α1A subunit, this variance being determined by the associated β subunits. This conclusion is based on biophysical and pharmacological measurements of the macroscopic α1A, α2δ supported barium currents when associated with different β subunits. Indeed both ω-Aga IVA and sFTX block preferentially the α1A, βIb combination with an ID_{50} smaller than α1A, β2a, and β3, which otherwise have similar current/voltage relations. We conclude that the βIb-associated current is the closest to the native P/Q type current and pharmacology. However, the relatively slow inactivation differentiates it from the rapidly inactivating Q current, making the α1A, βIb, α2δ the most likely candidate for the P current.

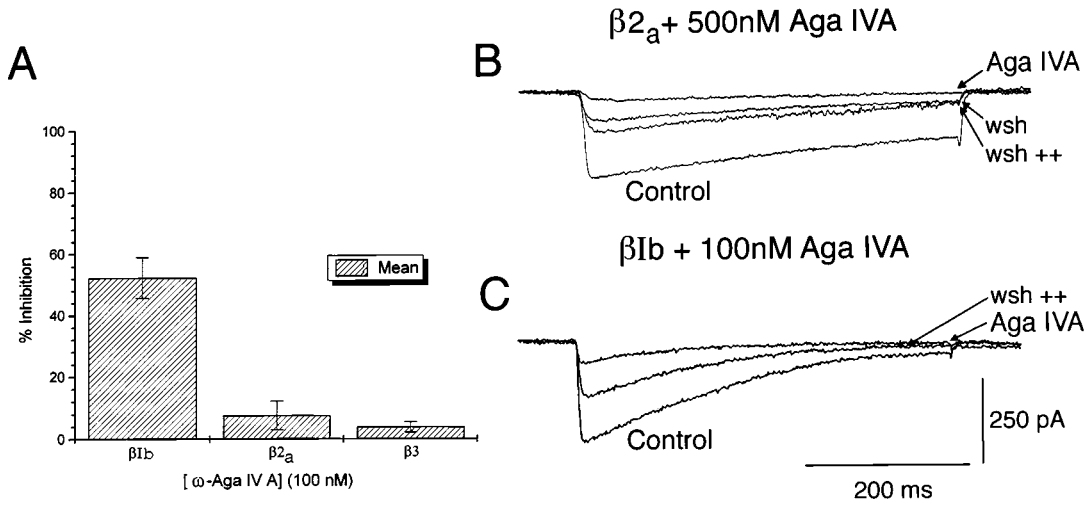

FIG. 4. ω-Aga IVA is a specific inhibitor of α1A, α2δ, βIb currents. (*A*) Comparison of the effect of 100 nM ω-Aga IVA after 8 min of constant local application on α1A, α2δ, βIb (βIb), α1A, α2δ, β_{2a} (β_{2a}) and α1A, α2δ, β3 (β3). (*B*) α1A, α2δ, β2a currents are inhibited by 500 nM ω-Aga IVA in a reversible fashion, washout (wsh) is increased on strong prepulse depolarizations (wsh++) (see text). (*C*) ω-Aga IVA effect on α1A, α2δ, βIb currents before (control) and after 100 nM Aga IVA, application (Aga IVA) and on toxin withdrawal and high depolarization protocol (wsh++).

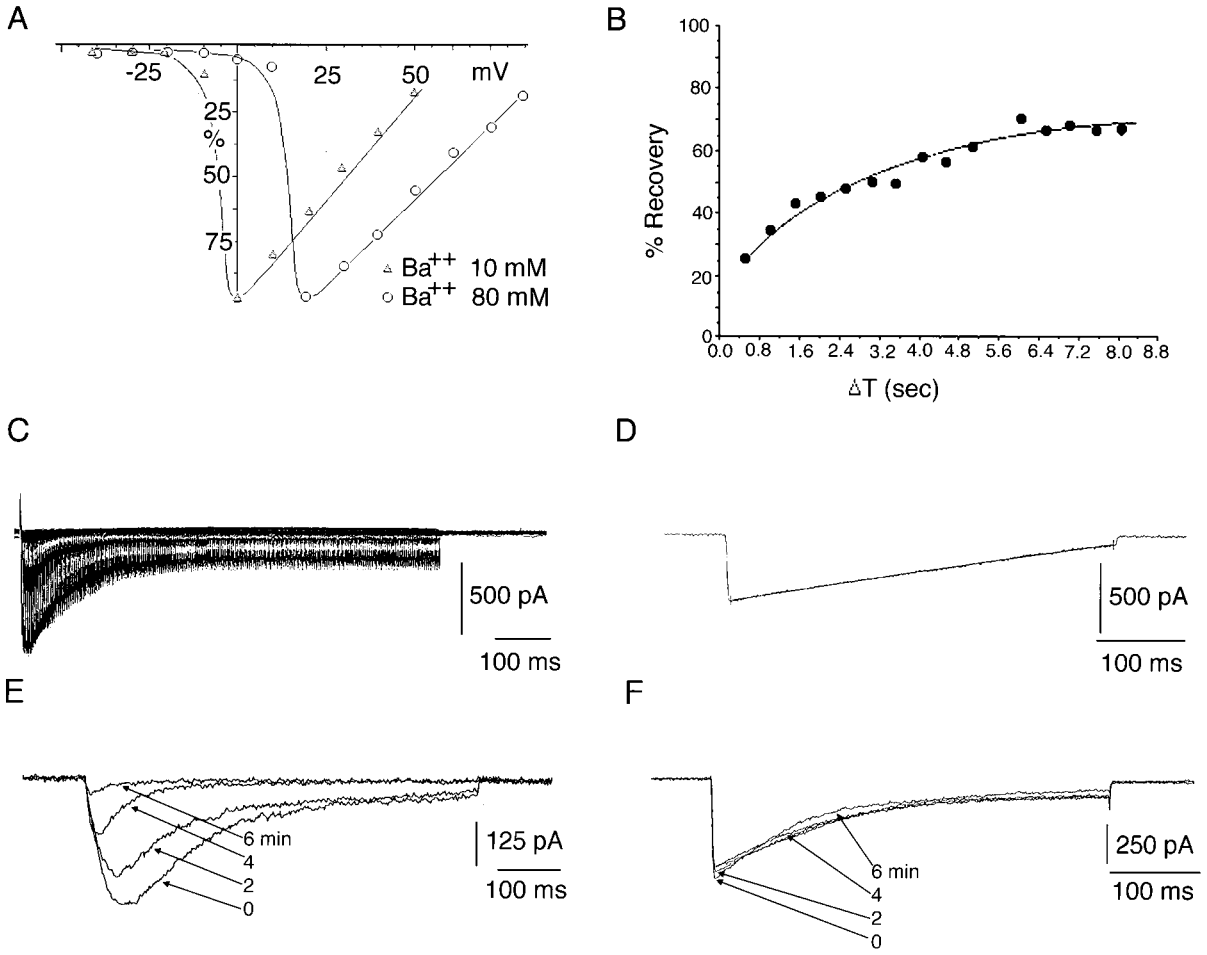

FIG. 5. α1A, α2δ, βIb currents characteristic features. (*A*) Comparison of *I–V* relations of α1A, α2δ, βIb currents in 10 (△) and 80 (○) mM barium. (*B*) Time course of recovery from inactivation of currents expressed by α1A, α2δ, βIb cDNAs. The currents were obtained during pairs of depolarizing pulses to +10 mV separated by intervals at −100 mV of increasing duration. The first interval was 40 msec and increments of 40 msec up to 8 sec. Recovery current is plotted as a function of time. (*C*) α1A, α2δ, βIb currents elicited by pulses to +60 mV from a holding potential of −90 mV. The pulse duration is incremented at 2 msec steps and delivered every 15 sec up to a maximum duration of 750 msec. This sequence generates a curve with an inactivation τ similar to the one observed with a single pulse to +10 mV and 500-msec duration in the same cell (*D*) Evidence of calcium-induced calcium current inhibition in currents generated by α1A, α2δ, βIb cDNAs. (*E*) Recordings of calcium currents (see *Material and Methods*) elicited by a depolarization to +10 mV from Vh = −90 mV delivered every 30 sec. Shown are currents obtained at control (0), 2, 4 and 6 min. (*F*) Same protocol and combination of cDNAs as in *E* but in 10 mM extracellular barium. The contrast of current stability between *E* and *F* is dramatic.

Whereas the biophysical results are in agreement with previous findings (5, 9, 10) the pharmacological results are unexpected, as they demonstrate that the β subunits influence the pharmacological properties of the current. Because the β subunit is an intracellular moiety the results suggest that this subunit must induce an allosteric change on the α1A subunit that modifies its pharmacological sensitivity. This conclusion touches on issues of channel characterization. It is apparent from present results that the association of the α1A, α2δ, βIb structure mimics the biophysical and pharmacological properties of classical P, and to a lesser extent the Q channels. Furthermore, it has been identified as P-type calcium channel of cerebellar granular neurons (19) with different functional properties from the initially described P-type calcium channel in Purkinje cells. The granule cell variant of the P channel shows slow inactivation kinetics reaching 34% inactivation at +10 mV after 720 msec. Expression of α1A, α2δ, βIb in COS cells (20) supports a slower inactivating I_{Ba} *I–V* shifted to the right as well as a lower apparent K_D (11 nM) for ω-Aga IVA, than the one reported in the present work. Nevertheless, the result supports the view that the combination α1A, α2δ, βIb as best replicating the properties of the native P-type channel. Concerning channel characterization the differences in the pharmacology and electrophysiological properties of α1A, βIb I_{Ba} in various heterologous expression systems (oocytes) (4, 5), COS cells (20), and HEK cells (present work) may reflect different cellular processing mechanism. Alternatively, they may be due to post-translational modifications and/or differences in the ionic strength used in the different preparations, because expression of the same α subunits with β3 in HEK cells (21) produced an *I–V* similar to the one found in this work.

Since the inhibition produced by ω-Aga IVA and sFTX on α1A, α2δ, β(s) currents reached a saturation level without total block and the classification of R-type calcium currents relies on the unblocked total calcium currents with a toxin cocktail, this finding opens the possibility that R-type current may represent one of the α1A, α2δ, β(s) combinations tested. This theme requires further experimentation.

In conclusion, the channels composed of α1A, α2δ, β-Ib are the most likely molecular counterpart of native P-type(s) channels. On the other hand, this structure does not reproduce the pharmacological properties of either P or Q channel exactly, as the sensitivity to sFTX and ω-Aga IVA for P-type channels is lower than for the α1A, α2δ, βIb channels in HEK

cells, whereas in COS cells (20) the IV curve is shifted to the right. This finding indicates that other elements may be lacking in HEK cells, preventing the exact reproduction of the native channel properties.

This work was supported by National Institutes of Health Grants NS13742 to R.L. and NS30989 to B.R.

1. Llinás, R., Sugimori, M., Lin, J.-W. & Cherksey, B. (1989) *Proc. Natl. Acad. Sci. USA* **86,** 1689–1693.
2. Mintz, I., Adams, M. & Bean, B. (1992) *Neuron* **9,** 85–95.
3. Randall, A. & Tsien, R. (1995) *J. Neurosci.* **15,** 2995–3012.
4. Zhang, J., Randall, A., Ellinor, P., Horne, W., Sather, W., Tanabe, T., Schwarz, T. & Tsien, R. (1993) *Neuropharmacology* **32,** 1075–1088.
5. Stea, A., Tomlinson, J., Soong, T., Bourinet, E., Dubel, S., Vincent, S. & Snutch, T. (1994) *Proc. Natl. Acad. Sci. USA* **91,** 10576–10580.
6. Mori, Y., Friedrich, T., Kim, M., Mikami, A., Nakai, J., Ruth, P., Bosse, E., Hofmann, F., Floreckerzi, V., Furuchi, J., Mikoshiba, K., Imoto, K., Tanabe, T. & Numa, S. (1991) *Nature (London)* **350,** 398–402.
7. Hofmann, F., Biel, M. & Flockerzi, V. (1994) *Annu. Rev. Neurosci.* **17,** 399–418.
8. Isom, L., DeJongh, K. & Catterall, W. (1994) *Nature (London)* **12,** 1183–1194.
9. Shistik, E., Ivanina, T., Puri, T., Hosey, M. & Dascal, N. (1995) *J. Physiol.* **481,** 55–62.
10. Sather, W., Tanabe, T., Zhang, J., Mori, Y., Adams, M. & Tsien, R. (1993) *Neuron* **11,** 291–303.
11. Gillard, S., Volsen, S., Smith, W., Beattie, R., Bleakman, D. & Lodge, D. (1997) *Physiol. Soc. Abst. Marine Biol. Assn.* 58.
12. Westenbroek, R., Sakurai, T., Elliot, E., Hell, J., Starr, T., Snutch, T. & Catterall, W. (1995) *J. Neurosci.* **15,** 6403–6418.
13. Day, N., Wood, S., Ince, P., Volsen, S., Smith, W., Slater, C. & Shaw, P. (1997) *J. Neurosci.* **17,** 6226–6235.
14. Hammill, A., Marty, A., Neher, E., Sakmann, B. & Sigworth, F. (1981) *Pflügers Arch.* **391,** 85–100.
15. Neher, E. (1992) *Methods Enzymol.* **207,** 123–131.
16. Lin, J.-W., Rudy, B. & Llinás, R. (1990) *Proc. Natl. Acad. Sci. USA* **87,** 4538–4542.
17. Cherksey, B., Sugimori, M. & Llinás, R. (1991) *Ann. N.Y. Acad. Sci.* **635,** 80–89.
18. Pearson, H., Sutton, K., Scott, R. & Dolphin, A. (1995) *J. Physiol.* **482,** 493–509.
19. Tottene, A., Moretti, A. & Pietrobon, D. (1996) *J. Neurosci.* **16,** 6353–6363.
20. Berrow, N., Brice, N., Tedder, I., Page, K. & Dolphin, C. (1997) *Eur. J. Neurosci.* **9,** 739–748.
21. Brody, D., Patil, P., Mulle, J., Snutch, T. & Yue, D. (1997) *J. Physiol.* **499,** 637–644.